Stepwise optimization of single-ion conducting polymer electrolytes for high-performance lithium-metal batteries

Xu Dong [a,b], Zhen Chen [a,b], Xinpei Gao [a,b], Alexander Mayer [a,b], Hai-Peng Liang [a,b], Stefano Passerini [a,b,*], Dominic Bresser [a,b,*]

[a] Helmholtz Institute Ulm (HIU), Helmholtzstrasse 11, 89081 Ulm, Germany
[b] Karlsruhe Institute of Technology (KIT), P.O. Box 3640, 76021 Karlsruhe, Germany

ARTICLE INFO

Keywords:
Single-ion conductor
Polymer electrolyte
Backbone chemistry
NCM_{622} cathode
Lithium-metal battery

ABSTRACT

Single-ion conducting polymer electrolytes (SIPEs) are promising candidates for high-energy and high-safety lithium-metal batteries (LMBs). However, their insufficient ionic conductivity and electrochemical stability hinder their practical application. Herein, three new SIPEs, *i.e.*, poly (1,4-phenylene ether ether sulfone)-Li (PEES-Li), polysulfone-Li (PSF-Li), and hexafluoropolysulfone-Li (6FPSF-Li), all containing covalently tethered perfluorinated ionic side chains, have been designed, synthesized, and compared to investigate the influence of the backbone chemistry and the concentration of the ionic group on their electrochemical properties and cell performance. Especially, the trifluoromethyl group in the backbone and the concentration of the ionic function appear to play an essential role for the charge transport and stability towards oxidation, and the combination of both yields the best-performing SIPE with high ionic conductivity of ca. 2.5×10^{-4} S cm^{-1}, anodic stability of more than 4.8 V, and the by far highest capacity retention in Li||$LiNi_{0.6}Co_{0.2}Mn_{0.2}O_2$ cells.

1. Introduction

The development of rechargeable lithium-metal batteries (LMBs) has attracted scientists and engineers since the 1970 s, owing to the high theoretical specific capacity (3,860 mA h g^{-1}) and the low negative electrochemical potential (3.04 V vs the standard hydrogen electrode) of metallic lithium [1–7]. However, in spite of a rapidly growing market, only lithium-ion batteries (LIBs) are widely employed now in portable electronic devices, (hybrid) electric vehicles (EVs), and stationary energy storage [8]; with only one exception: the polymer electrolyte-based Bolloré LMB technology operating at temperatures above 60 °C [9]. In fact, LMBs are still facing a few challenges for their further deployment. When using a liquid electrolyte, for example, capacity fading and safety hazards occur, caused by the Li dendrite growth [10–19]. In order to improve the cycling stability and safety of LMBs, solid polymer electrolytes are being intensively studied [20–28]. Compared with liquid electrolytes, they can alleviate most of the drawbacks of being poorly flammable, less toxic and more resistant to dendrite growth [29–32]. Among all, single-ion conducting polymer electrolytes (SIPEs) are considered appealing alternatives to conventional electrolytes, because they offer high thermal and chemical stabilities. Also they show lithium ion transference number close to unity, by which they can effectively suppress the growth of lithium dendrites, thus, improving the cycle life of the cell [22,33–37]. However, their usage has been hindered so far by insufficient ionic conductivity and/or limited electrochemical stability towards oxidation, preventing the combination with high-energy cathode materials such as $LiNi_{0.6}Co_{0.2}Mn_{0.2}O_2$ (NCM_{622}). Some SIPEs that have been reported earlier show, for instance, high ionic conductivity of more than 9.3×10^{-4} S cm^{-1} at 40 °C, but the relatively low electrochemical stability towards oxidation limits their use to lithium battery cells comprising $LiFePO_4$ (LFP) as the positive electrode active material [38–40]. Others show high ionic conductivity of more than 1.2×10^{-3} S cm^{-1} at 40 °C and the possibility to yield also stable cycling with NCM_{622} cathodes, but the synthesis procedure is more complex and, thus, requiring greater efforts for a potential scale-up [41,42]. Moreover, despite significant progress in the design principles for high-conductivity polymer electrolytes [41,43–51], the influence of the SIPE backbone chemistry and structure as well as the ionic group and its concentration on the electrochemical properties and cell performance

* Corresponding authors.
E-mail addresses: stefano.passerini@kit.edu (S. Passerini), dominic.bresser@kit.edu (D. Bresser).

requires further investigation. This is of great importance for the development of advanced polymer electrolytes for cost-efficient high-energy and high-safety LMBs.

Targeting an improved understanding of these impact factors, we compare herein three different SIPEs. The first one is based on poly(1,4-phenylene ether-ether-sulfone) (PEES), which is known to have good film-forming properties and high thermal resistance [52,53]. The sulfonyl group (i.e., sulfur is in the highest possible oxidation state) attracts electrons from the neighboring benzene rings, causing an electron deficiency and, hence, an increasing oxidation resistance. In combination with the aromatic groups and ether bonds in the PEES backbone, PEES thus provides the necessary strength, molecular rigidity, and good processability for the production of mechanically, chemically, and electrochemically stable membranes [54].

The second SIPE is based on polysulfone (PSF), which was chosen owing to its good thermal stability, film forming ability, and superior mechanical strength [55,56]. For these reasons, PSF is widely utilized, e.g., for the manufacturing of synthetic membranes for gas separation [57], ultra-filtration [58], ion exchange-membranes [59–61], polymer electrolyte membrane fuel cells [62], redox-flow batteries [63], and very recently also as artificial interphase for LMBs [64,65]. Moreover, there have already been efforts to prepare Li-ion conducting solid polymer electrolytes based on modified PSFs [66], however, the relatively strong-coordinating anionic species and insufficient room-temperature conductivity hinder their development. Compared to PEES, PSF offers one more brominated electrophilic reaction site in the polymer backbone, which enables the covalent linkage of two ionic functional groups per repeating unit rather than only one.

The third SIPE, hexafluoropolysulfone (6FPSF), is based on the two monomers 6F-bisphenol-A and bis(4-fluorophenyl)sulfone, and exhibits excellent thermal stability [67,68]. The intermediately formed polymer backbone also provides two reaction sites per repeating unit for a bromination reaction, which is then used for covalently tethering the ionic side chain. Furthermore, the -CF_3 groups in 6FPSF contribute to a reduced intersegmental chain packing and interaction, owing to the intermolecular repulsive forces between the fluorine atoms due to their high electron density [69]. In addition to the increased fractional free volume of the polymer, the fluorination leads to a relatively low dielectric constant and low water absorption, which renders such polymers favorable concerning their gas permeability and electronic isolation [70].

These three different kinds of polymers are functionalized with the same ionic side chain, i.e., lithium perfluorinated sulfonimide (-psiLi), yielding three SIPEs (Fig. 1) that are reported herein for the first time to the best of our knowledge. The three SIPEs have been comparatively investigated concerning their physicochemical and, especially, their electrochemical properties to derive important insights into the impact of the chemical structure of the backbone and the concentration of the ionic side chains. Eventually, all three SIPEs have been tested as electrolytes for Li||LFP and Li||NCM_{622} cells, evidencing the benefits of the trifluoromethyl groups in the backbone and the higher concentration of the lithiated side chain in 6FPSF-Li.

2. Experimental

2.1. Materials and synthesis

PEES, PSF, tetrafluoro-2-(tetrafluoro-2-iodoethoxy)ethanesulfonylfluoride ($ICF_2CF_2OCF_2CF_2SO_2F$, 97%), and EC were purchased from Sigma Aldrich. Trifluoromethansulfonamide ($CF_3SO_2NH_2$ 96%), anhydrous potassium carbonate (K_2CO_3, 98%), 4,4′-(hexafluor isopropyliden)diphenol ($(CF_3)_2C(C_6H_4OH)_2$, 98%), and copper powder (100 mesh, 99%) were purchased from Alfa Aesar. Triethylamine (TEA, 99.7%), bromine (Br_2, 99.5%), and bis(4-fluorphenyl) sulfone ($(FC_6H_4)_2SO_2$, 99%) were purchased from Acros Organics. 6FPSF was synthesized *via* a one-step polymerization reaction using 6F-bisphenol-A and bis(4-fluorophenyl)sulfone as the monomers. The covalent tethering of the -psiLi [41] side chains was conducted *via* a bromination of the polymer, followed by an Ullmann coupling reaction. The synthesis of all three ionomers is described in detail in the Supplementary Information, along with the corresponding ^{1}H NMR and ^{19}F NMR spectroscopy data.

2.2. Fabrication of the polymer membranes

To prepare the polymer electrolyte membranes of PEES-Li, PSF-Li, and 6FPSF-Li, the polymer powder was ground together with EC and deposited on Mylar films. Subsequently, these Mylar films were pressed *via* a hot press at 50 °C and 15 bar for 2 min. After

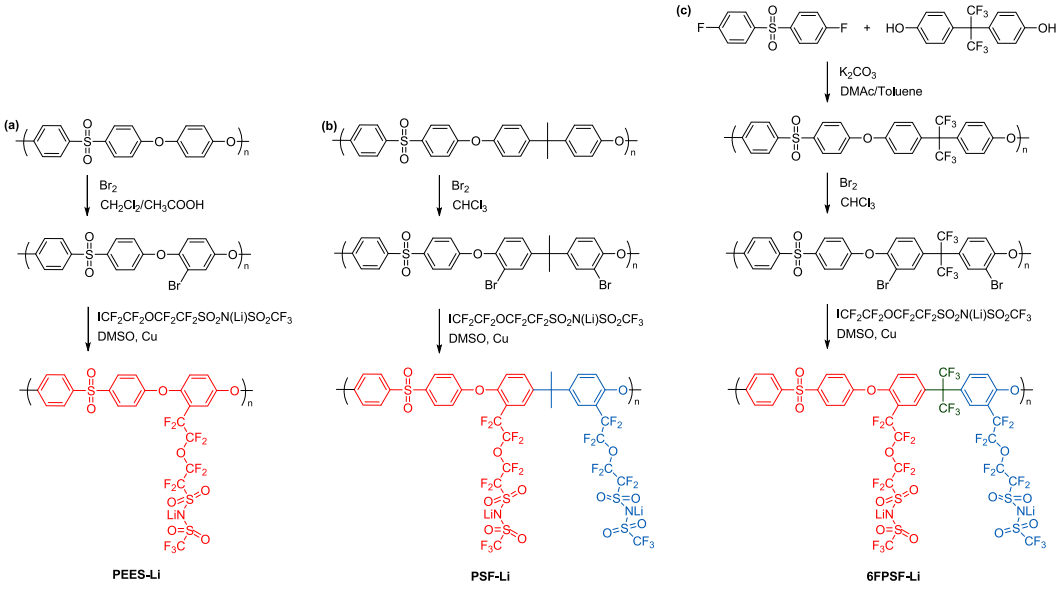

Fig. 1. Overview of the three SIPEs comparatively investigated herein and their synthesis: (a) PEES-Li, (b) PSF-Li, and (c) 6FPSF-Li.

cooling down to room temperature, they were hot-pressed twice more. All the dried polymer powder and membranes were stored and processed in the dry room with a dew point of less than 70 °C.

2.3. Thermal characterization

The thermal stability of the electrolytes was measured from 40 to 600 °C with a heating rate of 5 °C min^{-1} using a thermogravimetric analyzer under synthetic air (80% N_2 and 20% O_2) with a flow rate of 20 mL min^{-1}. These measurements were also used to determine the EC content in the polymer membranes. Differential scanning calorimetry (DSC) was performed for the identification of the glass transition temperature (T_g) and crystallinity of the samples. The measurement was conducted using 5 mg of sample in a sealed aluminum capsule under the continuous flow of dried and deoxygenated argon at 50 mL min^{-1}, and at a sweep rate of 5 °C min^{-1} from 100 to 150 °C and backwards. The heating step of the second cycle was used for the determination of the T_g.

2.4. Electrochemical characterization

The electrochemical stability of the electrolytes was investigated by linear sweep voltammetry (LSV) performed with pouch bag-type cells, which contained the electrolyte membranes sandwiched between lithium metal (Honjo, battery grade) and nickel foil, at a scan rate of 1.0 mV s^{-1} between 0.5 and 5.5 V and utilizing a VMP Biologic electrochemical workstation. The ionic conductivity of the polymer electrolytes was determined by electrochemical impedance spectroscopy (EIS) at various temperatures ranging from 20 to 80 °C using a Solartron impedance analyzer (SI 1260). For these experiments, the polymer electrolyte membranes were sandwiched between two copper foils and sealed in pouch bag-type cells inside the dry room. The cells were allowed to stabilize at a given temperature for 3 h prior to each measurement. The impedance spectra were taken in the frequency range from 0.01 Hz to 0.1 MHz with an AC amplitude of 10 mV. The bulk resistance of the membrane was determined as the intercept of the semicircle with the real axis in the Nyquist plot using the ZView software. The conductivity (σ) was calculated from Eq. (1).

$$\sigma = \frac{L}{R * S} \tag{1}$$

where R is the bulk membrane resistance, L is the thickness of the electrolyte membrane, and S is the electrode surface area.

The limiting current density was determined using symmetric Li||Li cells and the Solatron 1400 CellTest system at a constant sweep rate of 0.02 mV s^{-1}.

To investigate the interfacial stability between Li and the SIPEs, long-term galvanostatic lithium stripping and plating tests were performed at different current densities for symmetric Li||Li pouch cells using a Maccor S4000 battery tester.

The Li^+ transference number (t^+) was determined by combining chronoamperometry (CA) and EIS for symmetric Li||Li pouch cells according to the method reported by Bruce, Vincent and Evans [71,72]. The applied polarization (ΔV) was 10 mV. t^+ was calculated by Eq. (2).

$$t^+ = \frac{I_S(\Delta V - I_0 R_0)}{I_0(\Delta V - I_S R_S)} \tag{2}$$

where I_0 and I_S represent the initial and steady-state current, respectively. R_0 and R_S are the initial and steady-state resistance before and after the polarization process, respectively.

2.5. Electrode preparation and testing

LFP positive electrodes were composed of 80 wt% LFP, 10 wt% polyvinylidene fluoride (PVdF, Solvay; 4 wt%), and 10 wt% carbon black, cast on aluminum foil. After drying for 6 h at 80 °C, the coated aluminum foils were cut into 12 mm diameter disks, which were eventually dried at 120 °C for 10 h under vacuum. The areal loading of the LFP electrodes was 1.9 ± 0.1 mg cm^{-2}. The LFP|SIPE|Li cells were charged and discharged between 2.5 and 4.0 V at different current densities. The NCM_{622} cathodes consisted of 92 wt% NCM, 4 wt% PVdF, and 4 wt% carbon black coated on aluminum foil. After punching, the electrodes were subjected to air-drying at 80 °C for 6 h and vacuum drying at 120 °C for 10 h. The average active material mass loading was 2.3 ± 0.1 mg cm^{-2}. NCM_{622}|SIPE|Li cells were cycled between 3.0 and 4.2 V. A dis-/charge rate of 1C corresponds to a specific current of 170 mA g^{-1} for both active materials. The pouch cells were assembled in the dry room with a dew point of less than 70 °C. The tests were performed with a Maccor battery cycler at 40 °C.

3. Results and discussion

First, the amount of solvent to be incorporated in the SIPE was investigated to maximize the ionic conductivity while maintaining good mechanical properties. It was observed that solvent contents higher than 40 wt% led to extremely sticky and soft membranes, resulting in detrimental electrode|electrolyte interfaces upon cell assembly and, accordingly, inferior cell performance. Hence, an EC content of 40 wt% was chosen for all further tests. In the next step, different organic carbonates and carbonate mixtures were evaluated as potential "molecular transporters" by comparing their electrochemical stability after incorporation in the three different SIPEs (Fig. S1). While there is no clear trend concerning the anodic stability, it is apparent that the use of EC favors lithium plating, as indicated by the higher cathodic current. This is assigned to the higher dielectric constant of EC [21], which is beneficial for reducing the interaction between the anionic side chains and the Li cations, making the latter more mobile [73]. Hence, it was chosen as the most appropriate solvent in the given setup for further investigation of the polymer electrolytes. Fig. S2 shows photographs of the three SIPE membranes containing 40 wt% EC along with the determination of their thickness (all about 200 μm). The membranes show good flexibility, processability, and self-standing properties.

Subsequently, we looked at the ESW in more detail, now keeping the solvent the same, but comparing the different SIPEs in one plot (Fig. 2). The PEES-Li polymer electrolyte displays an ESW of 4.56 V vs Li^+/Li at 40 °C, considering a current flow of 20 μA cm^{-2} as the stability threshold. The ESW increases to 4.82 V and 4.96 V for 6FPSF-Li and PSF-Li, respectively (Fig. 2), which renders all of them as promising candidate electrolytes for the realization of high-voltage LMBs. The slightly lower anodic stability of 6FPSF-Li compared to PSF-Li is in line with previous observations concerning the incorporation of such $-CF_3$ groups and might be related to the formation of thermodynamically more stable decomposition products [74]. Besides, the tiny peak above 1.0 V in the cathodic scan indicates that there is a small amount of DMSO remaining in the ionomer from the synthesis procedure [75], and the additional feature below 1.0 V is ascribed to the reductive decomposition of EC [76]. The sharp current increase below 0 V is related to the deposition of metallic lithium, and among the three SIPEs, 6FPSF-Li shows a slightly steeper current increase, revealing faster deposition kinetics.

The thermal stability of the three materials was analyzed via TGA and the results obtained for three polymers as such and with

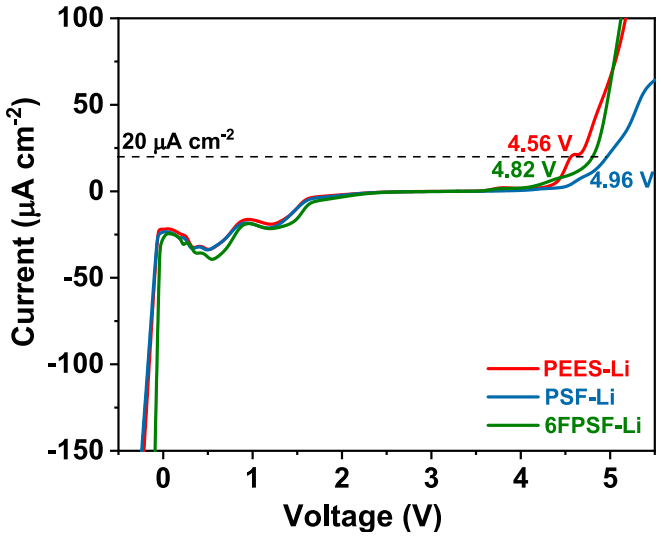

Fig. 2. Comparative determination of the electrochemical stability via linear sweep voltammetry of EC-doped PEES-Li, PSF-Li, and 6FPSF-Li at 40 °C (sweep rate: 1 mV s ^{1}; for each experiment, freshly assembled Li||Ni pouch-type cells were used).

40 wt% EC are presented in Fig. 3(a and b), respectively. The TGA curves of the polymer powders are very similar and almost overlapping at temperatures below 300 °C (Fig. 3a), indicating that the concentration of ionic functions (side chains) does not substantially affect the thermal stability of the dry ionomers. All polymers show very good thermal stability with less than 2.7% weight loss below 300 °C, which is well above the lithium melting point or the SEI degradation of graphite [32]. From Fig. 3(b), the evaporation of EC is seen to occur between around 150 and 250 °C, followed by the decomposition of the polymer. The PEES-Li electrolyte releases all EC at the lowest temperature as expected for the lowest number of ionic functions, i.e., the lowest interaction between the solvent and the ions. Among the other two SIPEs, 6FPSF-Li appears to show the slightly weaker interaction with solvent, presumably owing to the ionophobic nature of the $-CF_3$ groups. In fact, only PSF-Li shows an EC evaporation onset comparable to pure EC (Fig. S3), indicating that the molecular distribution of the solvent molecules in the SIPEs favors the evaporation if the interaction with the SIPE is not sufficiently strong to counterbalance this behavior.

In addition to the electrochemical and thermal stability, the ionic conductivity of the polymer electrolyte plays a critical role in improving the performance of LMBs. Fig. 4 displays the temperature dependency of the polymer electrolytes' ionic conductivity at various temperatures, ranging from 10 °C to 80 °C. The ionic conductivity of PEES-Li, PSF-Li, and 6FPSF-Li at 40 °C is 1.95×10^{-4} S cm^{-1}, 2.23×10^{-4} S cm^{-1}, and 2.46×10^{-4} S cm^{-1}, respectively. These conductivity values essentially reflect the Li^+ conductivity, as the lithium-ion transference numbers were determined to be 0.89 (PEES-Li), 0.93 (PSF-Li), and 0.93 (6FPSF-Li). The minor deviation from unity might result from the presence of smaller charged species (e.g., decomposition products resulting from the contact with lithium), the immediate formation of a charge-transport limiting interphase [77], or an initial reorganization at the interface. Generally, though, it is obvious that a higher concentration of Li^+ cations in the polymer electrolyte, resulting from higher contents of the ionic side chain, yields higher conductivities, as offered by PSF-Li and 6FPSF-Li.

The limiting current densities presented in Fig. 5 were obtained from symmetric Li||Li cells subjected to voltage scan at a sweep rate of 0.02 mV s^{-1} at a temperature of 40 °C. PEES-Li shows a limiting current density of 0.29 mA cm^{-2}, while PSF-Li and 6FPSF-Li showed a limiting current density of 0.64 mA cm^{-2}, i.e., slightly more than twice that of the former. This is ascribed to the essentially doubled Li^+ concentration, suggesting that there is a direct correlation between the two factors and implying a possibly higher rate performance of the latter two systems [78,79].

The dynamic interfacial stability between the polymer electrolytes and lithium-metal electrodes was investigated by lithium stripping/plating experiments performed on symmetric Li||Li cells (Fig. 6a-c). At a low current density of 0.005 mA cm^{-2}, PEES-Li, PSF-Li, and 6FPSF-Li exhibit an overpotential of 8, 7, and 5 mV, respectively.

The overpotential of 6FPSF-Li rises to 61 and 123 mV (Fig. 6c) at a current density of 0.05 and 0.1 mA cm^{-2}, respectively, which is somewhat lower than the increase in overpotential recorded for the other two electrolytes (see Table S1 for a complete overview). In all three cases, though, the overpotential increases linearly with an increasing current, following Ohm's law, and reversibly decreases when lowering the current density back to 0.005 mA cm^{-2}, demonstrating good compatibility with lithium-metal electrodes and a rather stable electrode|electrolyte interface and interphase. This is further corroborated by the Nyquist plots recorded continuously during a lithium stripping and plating

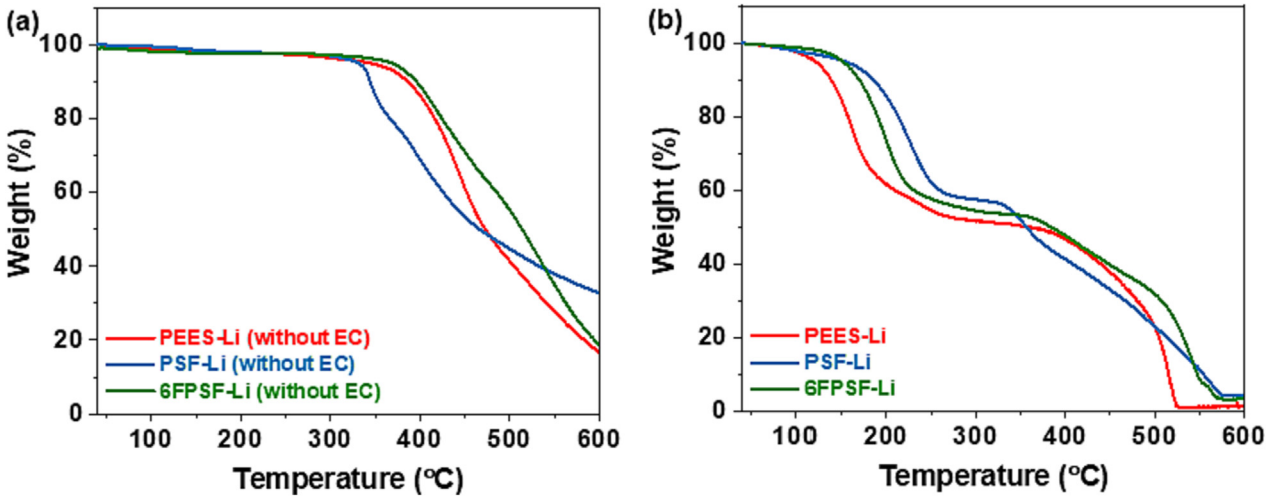

Fig. 3. Thermal analysis of (a) the dry and (b) the EC-doped ionomers. The heating ramp was 5 °C min ^{1} from 40 °C to 600 °C with a N_2/O_2 flow rate of 20 mL min ^{1}.

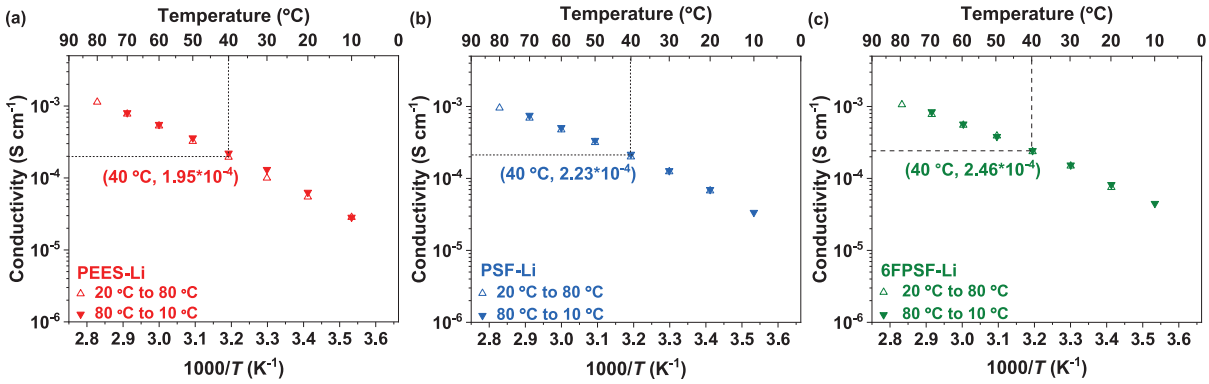

Fig. 4. Temperature-dependent ionic conductivity of the three polymer electrolytes: (a) PEES-Li, (b) PSF-Li, and (c) 6FPSF-Li. The ionic conductivity was recorded upon heating and cooling to confirm the reversibility of this analysis (frequency range: 0.01 Hz to 0.1 MHz, AC amplitude: 10 mV).

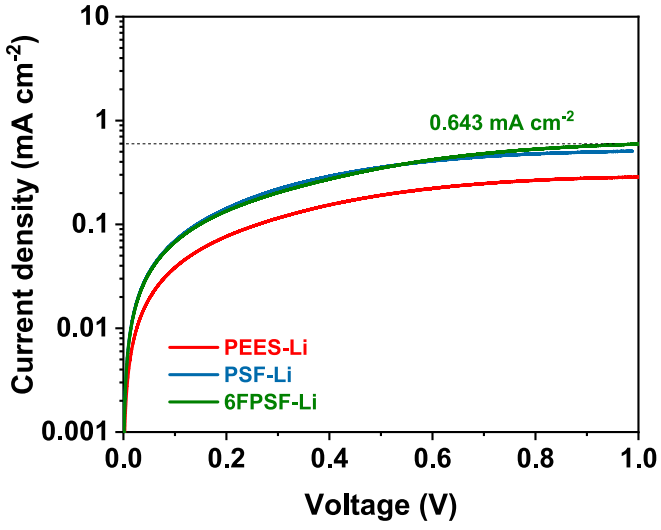

Fig. 5. Determination of the limiting current density of the three polymer-based electrolyte systems (sweep rate: 0.02 mV s ^{1}, temperature: 40 °C).

experiment at a constant current density of 0.05 mA cm^{-2} (Fig. 6d-f; see Fig. S4 and Table S2 along with a more detailed discussion of the findings in the Supporting Information). While these generally indicate a rather stable interface resistance, the minor fluctuations are well resembling the minor fluctuations observed for the overpotential at higher current densities in Fig. 6(a-c). PEES-Li, for instance, shows a steady (though minor) decrease (Fig. 6a and d), while 6FPSF-Li shows a minor increase initially, before it eventually stabilizes – both the overpotential (Fig. 6c) as well as the impedance (Fig. 6f). Overall, 6FPSF-Li shows the most promising electrochemical properties and behavior in contact with lithium-metal electrodes out of the three different electrolyte systems, presumably owing to the formation of an F-richer interphase owing to the incorporation of the additional fluorine.

To further investigate the impact of the backbone chemistry and charge concentration in the ionomer, Li||LFP and Li||NCM$_{622}$ cells were assembled and studied.

The rate performance upon galvanostatic cycling of the Li||LFP pouch cells is presented in Fig. 7(a). The cell discharge capacities delivered with the three electrolytes at low C rates are rather comparable ranging from about 157 mA h g^{-1} at 0.1C to about 140 mA h g^{-1} at 0.5C. At higher C rates, however, the cell employing 6FPSF-Li delivers capacities of about 129 mA h g^{-1} (1C) and 85 mA h g^{-1} (2C), which are much higher than those achieved with PEES-Li and PSF-Li. Especially at 2C, the cells employing these latter electrolytes deliver no capacity, in fact. The superior rate capability of the cells employing 6FPSF-Li may be attributed to the higher charge concentration and the lower interfacial charge transfer resistance owing to the presence of the trifluoromethyl groups which appear to have a beneficial impact in this regard. Indeed, the voltage profiles recorded at 1C (see Fig. 7b) show a lower polarization for the 6FPSF-Li-based cell compared to those recorded for the other electrolytes, corroborating that the internal cell impedance is the limiting factor at elevated rates. At lower rates, i.e., 0.1C, the Li||LFP cells deliver (very) stable cycling for more than 250 cycles (Fig. 7c), although the stability increases in the order PEES-Li < PSF-Li < 6FPSF-Li. This is also reflected by the highly reproducible and well-defined plateaus of the Li||LFP cell employing 6FPSF-Li, confirming the importance of a suitable charge carrier concentration and the advantageous presence of the –CF$_3$ groups (Fig. 7d).

The investigation of the Li||NCM$_{622}$ cells is presented in Fig. 8. Fig. 8(a) shows the rate performance of these cells at dis-/charge rates ranging from 0.05C to 1C. All electrolytes show a high specific capacity of approximately 160 mA h g^{-1} at 0.05C, with PEES-Li and PSF-Li showing a slightly higher capacity than 6FPSF-Li. As the dis-/charge rate is increased, however, the cell employing 6FPSF-Li shows higher specific capacities of 97 mA h g^{-1} and 54 mA h g^{-1} at 0.5C and 1C, respectively, while the cells employing the other two electrolytes only delivered a capacity of around 53 mA h g^{-1} and 0 mA h g^{-1} at the same C rates owing to the substantially higher polarization (Fig. 8b), presumably originating from superior charge transport kinetics at the interfaces in the case of 6FPSF-Li. Additionally, as shown in Fig. 8(c), the 6FPSF-Li-comprising Li||NCM$_{622}$ cells demonstrate excellent cycling stability at 0.2C with a capacity retention of around 83% after 250 charge/discharge cycles and an average CE of 99.6%. Differently, the cells employing PEES-Li and PSF-Li only provide capacity retention of 60.3% and 53.2% after 80 and 250 cycles, respectively. Fig. 8(d) presents the dis-/charge profiles of the 10th and 50th cycle for all three different cells, highlighting the increasing polarization in the order 6FPSF-Li < PSF-Li < PEES-Li. Particularly for 6FPSF-Li, the polarization and capacity fading are substantially less pronounced compared to the frequently observed capacity fading of NCM cathodes in combination with polymer-based electrolytes [80,81].

Overall, the results obtained from the Li||LFP and Li||NCM$_{622}$ cells demonstrate the superior electrochemical behavior of the 6FPSF-Li-based SIPE, resulting from its high ionic conductivity and limiting current density as well as the chemical and electrochemical stability, for which the higher charge concentration and the presence of the trifluoromethyl group appear to be very bene-

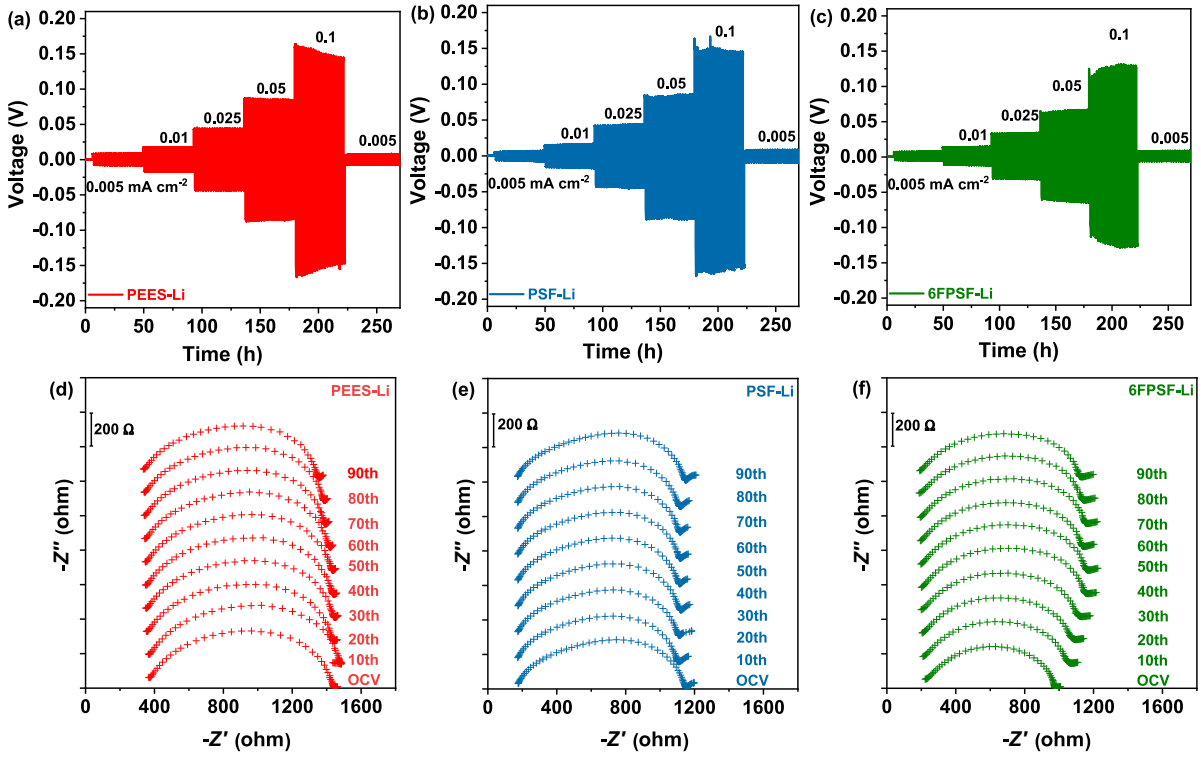

Fig. 6. (a-c) Lithium stripping and plating experiments conducted at varying current densities of 0.005, 0.01, 0.025, 0.05, and 0.1 mA cm ^{2} on symmetric Li||Li cells comprising (a) PEES-Li, (b) PSF-Li, and (c) 6FPSF-Li as the electrolyte (each stripping and plating step lasted for 1 h). (d-f) EIS spectra measured after every 10 stripping/plating cycles at 0.05 mA cm ^{2} and 40 °C for (d) PEES-Li, (e) PSF-Li, and (f) 6FPSF-Li.

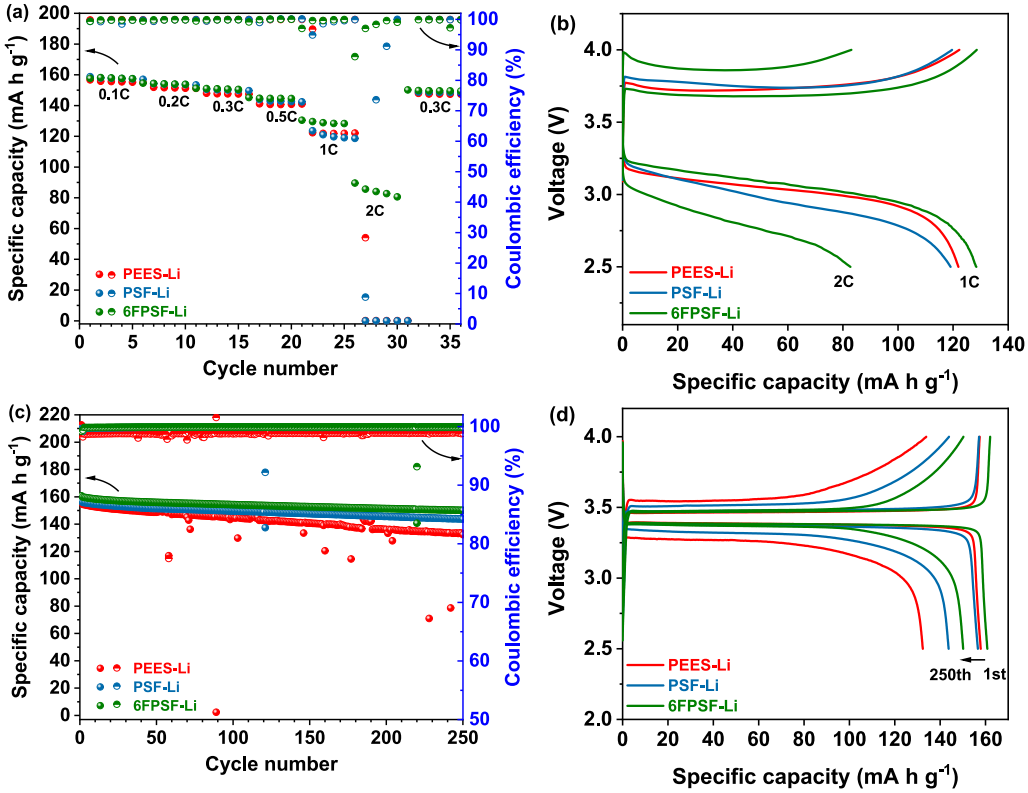

Fig. 7. Investigation of Li||LFP cells employing the three different SIPEs. (a) Rate performance tests and (b) the corresponding voltage profiles at 1C and 2C; (c) long-term galvanostatic cycling and (d) corresponding potential profiles for selected cycles; the first cycle was conducted at 0.05C, all following ones at 0.1C. The cut-off voltages were set to 2.5 and 4.0 V and the cells were kept at a constant temperature of 40 °C (1C = 170 mA g ^{1}).

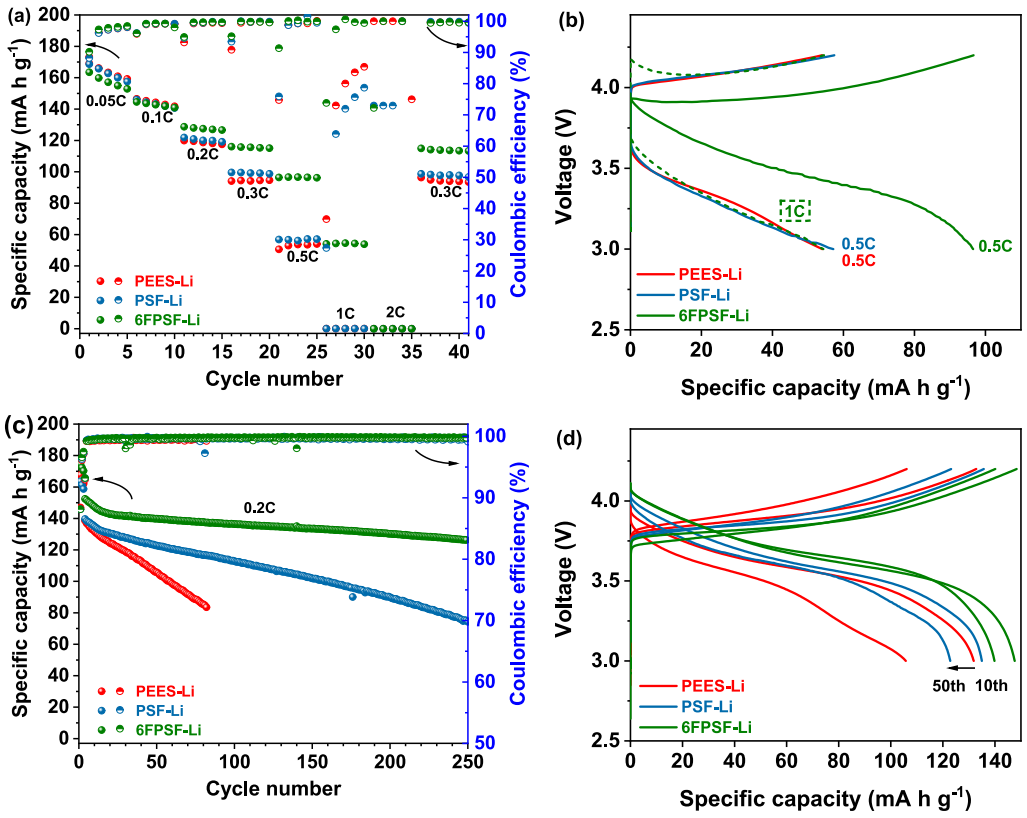

Fig. 8. Investigation of Li||NCM_{622} cells. (a) Rate performance and (b) the corresponding voltage profiles at 0.5C and 1C. (c) Long-term galvanostatic cycling and (d) the corresponding voltage profiles of the 10th and 50th cycle. The first three cycles were conducted at 0.05C and all following ones at 0.2C. The cut-off voltages were set to 3.0 and 4.2 V and the cells were kept at a constant temperature of 40 °C (1C = 170 mA g ^{1}).

ficial; with the latter allowing presumably for the formation of more stable and less resistive fluorine-richer interphases at the negative and positive electrode.

4. Conclusions

Three new polymer electrolytes consisting of covalently tethered -psiLi side chains to different polymer backbones were successfully synthesized and evaluated for application as SIPEs in LMBs. After introducing 40 wt% of EC, the polymer electrolytes offer high Li^+ ion conductivity, excellent thermal stability, and great performance in Li||LFP cells. Particularly, the 6FPSF-Li electrolyte, bearing trifluoromethyl groups in the polymer backbone and a higher content of the ionic side chains, offers superior charge transport in the bulk and across the electrode|electrolyte interfaces – for both lithium-metal anodes and NCM_{622} cathodes. The corresponding Li||NCM_{622} cells exhibit highly reversible specific capacities, good cycling stability, and very good rate performance. These results indicate that cell performance improvements may be substantially achieved by tailoring the chemical structure of the considered single-ion conducting polymer and increasing the concentration of the lithiated side chain(s), thus, highlighting the need for an in-depth understanding of the relevant impact factors for the design of high-performance polymer electrolytes.

Declaration of competing interest

The authors declare that they have no known competing financial interests or personal relationships that could have appeared to influence the work reported in this paper.

Acknowledgments

The authors gratefully acknowledge the financial support from the Federal Ministry of Education and Research (BMBF) within the FestBatt project (03XP0175B) and the FB2-Poly project (03XP0429B). Additionally, the authors acknowledge the financial support from the Helmholtz Association.

References

[1] P.G. Bruce, S.A. Freunberger, L.J. Hardwick, J.-M. Tarascon, Nat. Mater. 11 (2012) 19.
[2] X. Ji, L.F. Nazar, J. Mater. Chem. A 20 (2010) 9821–9826.
[3] M.S. Whittingham, Proc. IEEE Inst. Electr. Electron. Eng. 100 (2012) 1518–1534.
[4] W. Xu, J. Wang, F. Ding, X. Chen, E. Nasybulin, Y. Zhang, J.-G. Zhang, Energy Environ. Sci. 7 (2014) 513–537.
[5] B. Horstmann, J. Shi, R. Amine, M. Werres, X. He, H. Jia, F. Hausen, I. Cekic-Laskovic, S. Wiemers-Meyer, J. Lopez, Energy Environ. Sci. 14 (2021) 5289–5314.
[6] F. Zhao, Q. Sun, C. Yu, S. Zhang, K. Adair, S. Wang, Y. Liu, Y. Zhao, J. Liang, C. Wang, ACS Energy Lett. 5 (2020) 1035–1043.
[7] J. Holoubek, M. Yu, S. Yu, M. Li, Z. Wu, D. Xia, P. Bhaladhare, M.S. Gonzalez, T.A. Pascal, P. Liu, ACS Energy Lett. 5 (2020) 1438–1447.
[8] M. Armand, P. Axmann, D. Bresser, M. Copley, K. Edström, C. Ekberg, D. Guyomard, B. Lestriez, P. Novák, M. Petranikova, J. Power Sources 479 (2020).
[9] P. Hovington, M. Lagacé, A. Guerfi, P. Bouchard, A. Mauger, C. Julien, M. Armand, K. Zaghib, Nano Lett. 15 (2015) 2671–2678.
[10] C.-P. Yang, Y.-X. Yin, S.-F. Zhang, N.-W. Li, Y.-G. Guo, Nat. commun. 6 (2015) 1–9.
[11] W. Luo, L. Zhou, K. Fu, Z. Yang, J. Wan, M. Manno, Y. Yao, H. Zhu, B. Yang, L. Hu, Nano Lett. 15 (2015) 6149–6154.

[12] R. Zhang, X.R. Chen, X. Chen, X.B. Cheng, X.Q. Zhang, C. Yan, Q. Zhang, Angew. Chem. Int. Ed. Engl. 129 (2017) 7872–7876.
[13] L.-C. Zeng, W.-H. Li, Y. Jiang, Y. Yu, Rare Metals 36 (2017) 339–364.
[14] D. Aurbach, E. Zinigrad, Y. Cohen, H. Teller, Solid State Ion 148 (2002) 405–416.
[15] R. Bhattacharyya, B. Key, H. Chen, A.S. Best, A.F. Hollenkamp, C.P. Grey, Nat. mater. 9 (2010) 504–510.
[16] K.J. Harry, D.T. Hallinan, D.Y. Parkinson, A.A. MacDowell, N.P. Balsara, Nat. mater. 13 (2014) 69–73.
[17] J.W. Choi, D. Aurbach, Nat. Rev. Mater. 1 (2016) 1–16.
[18] X. He, D. Bresser, S. Passerini, F. Baakes, U. Krewer, J. Lopez, C.T. Mallia, Y. Shao-Horn, I. Cekic-Laskovic, S. Wiemers-Meyer, Nat. Rev. Mater. 6 (2021) 1036–1052.
[19] Z.Y. Wang, Z.X. Lu, W. Guo, Q. Luo, Y.H. Yin, X.B. Liu, Y.S. Li, B.Y. Xia, Z.P. Wu, Adv. Mater. 33 (2021) 2006702.
[20] J.-H. Shin, W.A. Henderson, S. Passerini, ECS Solid State Lett. 8 (2005) A125.
[21] L. Long, S. Wang, M. Xiao, Y. Meng, J. Mater. Chem. A 4 (2016) 10038–10069.
[22] H. Zhang, C. Li, M. Piszcz, E. Coya, T. Rojo, L.M. Rodriguez-Martinez, M. Armand, Z. Zhou, Chem. Soc. Rev. 46 (2017) 797–815.
[23] Z. Tu, P. Nath, Y. Lu, M.D. Tikekar, L.A. Archer, Acc. Chem. Res. 48 (2015) 2947–2956.
[24] Z. Lin, X. Guo, H. Yu, Nano Energy 41 (2017) 646–653.
[25] M.A. Ratner, P. Johansson, D.F. Shriver, Mrs Bull. 25 (2000) 31–37.
[26] N. Balsara, D. Hallinan, Annu. Rev. Mater. Res 43 (2013) 503–525.
[27] A. Mayer, D. Steinle, S. Passerini, D. Bresser, Nanotechnology 33 (2021).
[28] H. Yuan, J. Luan, Z. Yang, J. Zhang, Y. Wu, Z. Lu, H. Liu, A.C.S. Appl, Mater. Interfaces 12 (2020) 7249–7256.
[29] J.-M. Tarascon, M. Armand, Issues and challenges facing rechargeable lithium batteries, Materials for sustainable energy: a collection of peer-reviewed research and review articles from, Nature Publishing Group, World Scientific, 2011, pp. 171–179.
[30] E. Quartarone, P. Mustarelli, Chem. Soc. Rev. 40 (2011) 2525–2540.
[31] A. Manthiram, X. Yu, S. Wang, Nat. Rev. Mater. 2 (2017) 1–16.
[32] J. Kalhoff, G.G. Eshetu, D. Bresser, S. Passerini, ChemSusChem 8 (2015) 2154–2175.
[33] M.D. Tikekar, S. Choudhury, Z. Tu, L.A. Archer, Nat. Energy 1 (2016) 1–7.
[34] W. Cai, Y. Zhang, J. Li, Y. Sun, H. Cheng, ChemSusChem 7 (2014) 1063–1067.
[35] G. Luo, B. Yuan, T. Guan, F. Cheng, W. Zhang, J. Chen, A.C.S. Appl, Energy Mater. 2 (2019) 3028–3034.
[36] D. Du, X. Hu, D. Zeng, Y. Zhang, Y. Sun, J. Li, H. Cheng, A.C.S. Appl, Energy Mater. 3 (2019) 1128–1138.
[37] J. Zhu, Z. Zhang, S. Zhao, A.S. Westover, I. Belharouak, P.F. Cao, Adv. Energy Mater. 11 (2021) 2003836.
[38] C. Li, B. Qin, Y. Zhang, A. Varzi, S. Passerini, J. Wang, J. Dong, D. Zeng, Z. Liu, H. Cheng, Adv. Energy Mater. 9 (2019) 1803422.
[39] Y. Zhang, Y. Chen, Y. Liu, B. Qin, Z. Yang, Y. Sun, D. Zeng, S. Passerini, Z. Liu, H. Cheng, J. Power Sources 397 (2018) 79–86.
[40] B. Qin, S. Jeong, H. Zhang, U. Ulissi, D. Vieira Carvalho, A. Varzi, S. Passerini, ChemSusChem 12 (2019) 208–212.
[41] H.-D. Nguyen, G.-T. Kim, J. Shi, E. Paillard, P. Judeinstein, S. Lyonnard, D. Bresser, C. Iojoiu, Energy Environ. Sci. 11 (2018) 3298–3309.
[42] D. Steinle, Z. Chen, H.-D. Nguyen, M. Kuenzel, C. Iojoiu, S. Passerini, D. Bresser, J. Solid State Electrochem 26 (2022) 97–102.
[43] R. Hooper, L.J. Lyons, M.K. Mapes, D. Schumacher, D.A. Moline, R. West, Macromolecules 34 (2001) 931–936.
[44] Y. Wang, F. Fan, A.L. Agapov, X. Yu, K. Hong, J. Mays, A.P. Sokolov, Solid State Ion 262 (2014) 782–784.
[45] M.A. Webb, Y. Jung, D.M. Pesko, B.M. Savoie, U. Yamamoto, G.W. Coates, N.P. Balsara, Z.-G. Wang, T.F. Miller III, ACS Cent. Sci. 1 (2015) 198–205.
[46] R. Khurana, J.L. Schaefer, L.A. Archer, G.W. Coates, J. Am. Chem. Soc. 136 (2014) 7395–7402.
[47] R. Spindler, D. Shriver, J. Am. Chem. Soc. 110 (1988) 3036–3043.
[48] N.S. Schauser, D.J. Grzetic, T. Tabassum, G.A. Kliegle, M.L. Le, E.M. Susca, S. Antoine, T.J. Keller, K.T. Delaney, S. Han, J. Am. Chem. Soc. 142 (2020) 7055–7065.
[49] Z. Chen, D. Steinle, H.-D. Nguyen, J.-K. Kim, A. Mayer, J. Shi, E. Paillard, C. Iojoiu, S. Passerini, D. Bresser, Nano Energy 77 (2020).
[50] D. Bresser, S. Lyonnard, C. Iojoiu, L. Picard, S. Passerini, Mol. Syst. Des. Eng. 4 (2019) 779–792.
[51] A. Mayer, H.-D. Nguyen, A. Mariani, T. Diemant, S. Lyonnard, C. Iojoiu, S. Passerini, D. Bresser, ACS Macro Lett. 11 (2022) 982–990.
[52] S. Mishra, S. Sachan, P. Mishra, Int. J. Environ. Res. Dev 4 (2014) 147–152.
[53] E. Unveren, T. Inan, S. Çelebi, Fuel Cells 13 (2013) 862–872.
[54] P. Maheswari, P. Barghava, D. Mohan, J. Polym. Res. 20 (2013) 74.
[55] Q. Lu, J. Fang, J. Yang, G. Yan, S. Liu, J. Wang, J. Membr. Sci. 425 (2013) 105–112.
[56] W.F. Hale, A.G. Farnham, R.N. Johnson, R.A. Clendinning, J Polym Sci A 1 (1967) 2399–2414.
[57] B. Zornoza, S. Irusta, C. Tellez, J. Coronas, Langmuir 25 (2009) 5903–5909.
[58] H. Susanto, M. Ulbricht, J. Membr. Sci. 327 (2009) 125–135.
[59] J.J. Min-suk, J. Parrondo, C.G. Arges, V. Ramani, J. Mater. Chem. A 1 (2013) 10458–10464.
[60] Z. Yuan, X. Li, Y. Zhao, H. Zhang, A.C.S. Appl, Mater. Interfaces 7 (2015) 19446–19454.
[61] S. Vico, B. Palys, C. Buess-Herman, Langmuir 19 (2003) 3282–3287.
[62] J. Yang, Q. Li, J.O. Jensen, C. Pan, L.N. Cleemann, N.J. Bjerrum, R. He, J. Power Sources 205 (2012) 114–121.
[63] B.P. Gindt, D.G. Abebe, Z.J. Tang, M.B. Lindsey, J. Chen, R.A. Elgammal, T.A. Zawodzinski, T. Fujiwara, J. Mater. Chem. A 4 (2016) 4288–4295.
[64] C. Dong, Z. Lin, Y. Yin, Y. Qiao, W. Wang, Q. Wu, C. Yang, D. Rooney, C. Fan, K. Sun, J. Energy Chem. 55 (2021) 1–9.
[65] Y. Ma, C. Dong, Q. Yang, Y. Yin, X. Bai, S. Zhen, C. Fan, K. Sun, J. Energy Chem. 42 (2020) 49–55.
[66] S. Guhathakurta, K. Min, Polymer 51 (2010) 211–221.
[67] J. McHattie, W. Koros, D. Paul, Polymer 32 (1991) 2618–2625.
[68] Z. Wang, T. Chen, J. Xu, Polymer Int 50 (2001) 249–255.
[69] Y. Dai, M.D. Guiver, G.P. Robertson, Y.S. Kang, K.J. Lee, Macromolecules 36 (2003) 6807–6816.
[70] S. Banerjee, G. Maier, M. Burger, Macromolecules 32 (1999) 4279–4289.
[71] J. Evans, C.A. Vincent, P.G. Bruce, Polymer 28 (1987) 2324–2328.
[72] P.G. Bruce, J. Evans, C.A. Vincent, Solid State Ion 28 (1988) 918–922.
[73] K. Xu, Chem. Rev. 104 (2004) 4303–4418.
[74] C. Iojoiu, Y. Shao, J. Solier, H.-D. Nguyen, H.P.K. Ngo, T. Berteaux, G. Vansse, D. Bresser, 50eme Colloque National du GFP, 2022.
[75] Y. Yamada, Y. Takazawa, K. Miyazaki, T. Abe, J. Phys. Chem. C 114 (2010) 11680–11685.
[76] X. Zhang, R. Kostecki, T.J. Richardson, J.K. Pugh, P.N. Ross Jr, J. Electrochem. Soc. 148 (2001) A1341.
[77] K. Borzutzki, J.R. Nair, M. Winter, G. Brunklaus, A.C.S. Appl, Mater. Interfaces 14 (2022) 5211–5222.
[78] J.-W. Park, K. Yoshida, N. Tachikawa, K. Dokko, M. Watanabe, J. Power Sources 196 (2011) 2264–2268.
[79] J.A. Maslyn, L. Frenck, V.D. Veeraraghavan, A. Mu̎ller, A.S. Ho, N. Marwaha, W.S. Loo, D.Y. Parkinson, A.M. Minor, N.P. Balsara, Macromolecules 54 (2021) 4010–4022.
[80] M. Wetjen, G.-T. Kim, M. Joost, G.B. Appetecchi, M. Winter, S. Passerini, J. Power Sources 246 (2014) 846–857.
[81] Y. Lin, Y. Cheng, J. Li, J.D. Miller, J. Liu, X. Wang, RSC Adv. 7 (2017) 24856–24863.